published by Ural Federal University
eISSN 2411-1414
chimicatechnoacta.ru

ARTICLE
2024, vol. 11(4), No. 202411415
DOI: 10.15826/chimtech.2024.11.4.15

Novel biosorbents based on carboxyethyl chitosan for Allura Red dye contaminated water treatment

Aleksandr A. Drannikov [a] *, Elena A. Blinova [a], Anastasya V. Korel [a], Alexander G. Samokhin [a], Polina I. Dubovskaya [a], Daria V. Lazurenko [b], Ekaterina O. Zemlyakova [c], Alexander V. Pestov [c], Ekaterina A. Litvinova [a]

a: Faculty of Physical Engineering, Novosibirsk State Technical University, Novosibirsk 630073, Russia
b: Faculty of Mechanical Engineering and Technologies, Novosibirsk State Technical University, 630073 Novosibirsk, Russia
c: I. Ya. Postovsky Institute of Organic Synthesis, Ural Branch of the Russian Academy of Sciences, 620990 Ekaterinburg, Russia
* Corresponding author: drannikov@corp.nstu.ru

This paper belongs to a Regular Issue.

Abstract

Low biodegradability of several dyes leads to their accumulation in water, causing ecological and health damage. The adsorption and, in particular, biosorption processes are widely applied for the wastewater treatment. This article presents the first comparative study of the Allura red dye removal under neutral pH at 25 °C applying novel biosorbents: carboxyethyl chitosan hydrogel (CEC) and cryogel of carboxyethyl chitosan cross-linked with butanediol-1,4 diglycidyl ether (DEB-CEC). The gels were synthesized in "green" manner, and the characterization revealed porous structure and high swelling for both biopolymer compositions, which are the properties important for adsorption. The kinetic studies demonstrated that the adsorption rate for DEB-CEC is better represented by pseudo-second-order, while CEC followed better pseudo-first-order kinetics. The adsorption isotherm of Allura Red suited the Temkin model for both samples, with the maximum adsorption capacity of 22.523 mg/g (45.4 μmol/g) and 10.482 mg/g (21.1 μmol/g) for CEC and DEB-CEC, respectively. The results demonstrated that CEC and DEB-CEC polymers can be used as biodegradable and eco-friendly biosorbents for Allura Red dye removal from aqueous solutions, making these biosorbents promising for wastewater treatment and prevention of the azo-dye environmental pollution.

Keywords

carboxyethyl chitosan
cross-linking
cryogel
biosorption
allura red
E129
water treatment

Received: 15.10.24
Revised: 10.11.24
Accepted: 12.11.24
Available online: 22.11.24

Key findings

- Adsorption process of Allura Red dye for CEC and DEB-CEC fits pseudo-first-order and pseudo-second-order kinetic models, respectively.
- Maximum adsorption capacity of 22.523 mg/g (45.4 μmol/g) and 10.482 mg/g (21.1 μmol/g) was determined for CEC and DEB-CEC, respectively.
- The adsorption isotherm of Allura Red suited the Temkin model for both biosorbents.

© 2024, the Authors. This article is published in open access under the terms and conditions of the Creative Commons Attribution (CC BY) license (http://creativecommons.org/licenses/by/4.0/).

1. Introduction

Sustainable development requires modern approaches to recover natural resources used for industrial purposes. In this context, lack of pure water appears to be crucial for humanity, threatening millions of lives worldwide. Pollution is generally caused by industries actively applying heavy metals, dyes, plastics, oil products and surfactants [1–3].

Dye-containing wastewater with a pollutant concentration ranging typically from 100 to 250 mg/L is discharged either from plants or from households in an amount of 50,000 tons annually. It has become a global problem pushing the development of water treatment techniques forward

[4]. Most dyes are synthetically derived, and they are able to penetrate the environment, predominately contaminating water, demonstrating low biodegradability and high accumulation ability [5, 6]. Some dyes are harmful for biological objects and humans causing toxicological [7], carcinogenic effects [8, 9], hypersensitivity reactions [10], allergic reactions [11], behavioral and neurocognitive effects [12]. About 60–70% of dyes are azo dyes, characterized by the presence in their structure of a chromophore group (–N=N–) conjugated with aryl radicals [13].

According to classification, Allura Red AC, also known as FD&C Red 40 or E129, is the monoazo dye [4]. It is presented in the form of dark red powder or granules obtained through diazo coupling of aminomethyl toluenesulfonic acid with naphthol sulfonic acid [14]. The structural formula of Allura Red AC is shown in Figure 1.

Back in 1980 the Joint Food and Agriculture Organization of the United Nations and the World Health Organization Expert Committee on Food Additives established the tolerable daily intake of Allura Red AC in the range of 0–7 mg/kg body weight/day, later approved by the EU Scientific Committee on Foods in 1984 and 1989, and remained unchanged since then [15]. At the same time, it was reported that in vivo Allura Red AC causes the DNA damage in the colon at an uptake level of 10 mg/kg body weight 3 hours after administration in pregnant mice, which was confirmed by the Comet assay [16]. No damaged DNA was observed in other organs or the embryo. At a dose equivalent to the accepted daily allowance (7 mg/kg) Allura Red AC promotes DNA damage in the colon cells in vitro and in vivo [17]. It was also reported that the combination of E129 with preservative sodium benzoate results in hyperactivity among children aged 8 to 9 years [18]. Moreover, Allura Red AC had a neurotoxicity effect on rats in both low (7 mg/kg/day) and high (70 mg/kg/day) doses, which was causes impairment in spatial learning, memory and rats' medial prefrontal cortex structure [19].

Across the years, dye release into the environment remains a global challenge, causing environmental and social dangers. The presence of dyes in water severely declines the chemical and physical water quality; it has an adverse effect on aquatic organisms and can lead to the inhibition of biological systems by causing a scarcity of light.

Many techniques were developed in order to remove the dye pollutants from water, including membrane filtration, ozonation, coagulation/flocculation, electrochemical oxidation and adsorption [20].

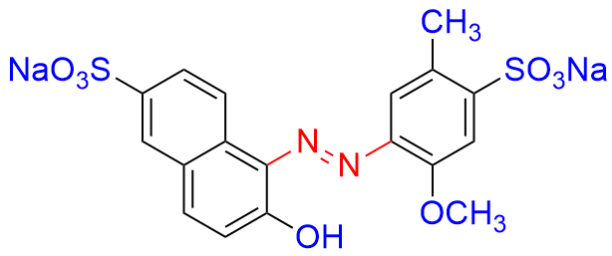

Figure 1 Structure of Allura Red AC.

Generally, the adsorption is considered to be the most cost-effective and simple approach [21], involving either conventional adsorbents such as carbon materials [22, 23], mineral adsorbents [24], chemical waste derived product [25], biomass [26, 27] or food waste [28] as well as wood sawdust [29] or biosorbents, such as alginate [30] or chitosan [31]. The adsorption parameters for some of these objects towards Allura Red AC are presented in Table 1.

According to the data in Table 1, biosorbents exhibit strong adsorption properties towards E129, which makes its use promising for dye removal. This follows the current trends in biosorbent application and their potential to displace carbon and other conventional adsorbents [39].

The biosorbents are especially attractive due to their modification capacity so that one can target the adsorption properties making the adsorbent more selective and efficient [40]. Another benefit of using biopolymers is their ease of processing; hence, the modifications can be carried out by various methods, including mechanical and thermal processes to create pores and chemical processes to improve the surface area [41]. This approach also reveals the potential for plant waste valorization by isolating biopolymers from biomass and producing renewable substances applying green technologies [42].

In the context of Allura Red adsorption, chitosan demonstrated perfect adsorption capacity compared to inert adsorbents due to the specific adsorption mechanism of chitosan. This amino-polysaccharide contains both hydroxyl and amine groups in its structure, which allows enhanced adsorption due to acid-base interactions or the formation of hydrogen bonds (Figure 2) [33].

Table 1 Allura Red AC adsorption depending on the sorbent.

Sorbent	Adsorption capacity, μmol/g	Adsorption conditions		Ref.
		T, °C	pH	
Bilghia sapida seed pods	30.55	26	4	[32]
Sawdust (microsized)	50.98	25	3	[29]
Activated carbon	146.75	25	7	[23]
Sawdust (nanosized)	151.46	25	3	[29]
Modified clays	121.77	25	5	[24]
Biosponges of chitosan cross-linked with epichlorohydrin supported by *Luffa cylindrica*	122.7	25	2	[33]
Biosponges of chitosan cross-linked with glutaraldehyde supported by *Luffa cylindrica*	179.38	25	2	[33]
Chitosan/Polyurethane foam	217	25	-	[34]
Pseudoevernia furfuracea biomass	221	25	8	[35]
Chitosan	604.33	25	5.7	[36]
Chitosan nanoparticles and beads cross-linked with sodium tripolyphosphate	746.07	25	4	[37]
Spirulina platensis	944	25	4	[38]

 DOI: 10.15826/chimtech.2024.11.4.15

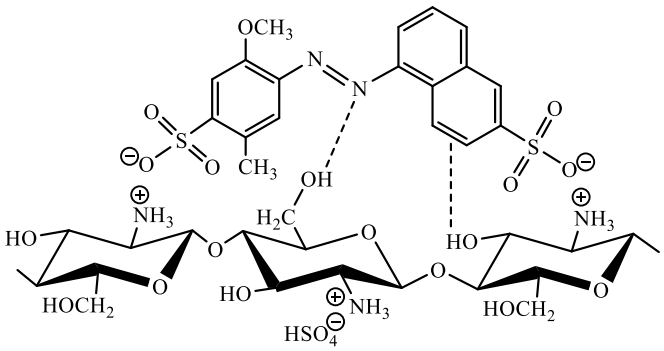

Figure 2 Pathways of interaction between chitosan and Allura Red dye.

Moreover, Figure 2 demonstrates high adsorption dependence on the pH due to the activation of different groups of chitosan and Allura Red dye. A number of publications for various azo dyes proves this statement. It's proved that low pH stimulates the adsorption, while it demonstrates a downward trend upon pH increase, reaching the values of adsorption capacity of about 50 for native chitosan [36, 43, 44].

Besides its numerous benefits such as renewability, low cost and toxicity, reusability, extended life cycle and rabid adsorption kinetics, chitosan requires its structure modification to enhance adsorption [45]. The modification usually represents incorporating additional chemical groups into the chitosan backbone. In most cases derivatization is carried out via amino-groups in such chemical reactions as acetylation, quaternization, Schiff base formation with aldehydes and ketones, alkylation, and carboxyalkylation [35]. Another approach is cross-linking, which allows forming the three-dimensional network by covalent bonds between linear chains of chitosan, enlarging the contact surface and providing biosorbents with a high capacity towards dyes in water [46]. Both derivatization and cross-linking affect the adsorption mechanisms involving physical adsorption or chemical interactions, such as ion-exchange, acid–base interactions, and hydrogen bonding [47].

In the present work, we made the first attempt to evaluate the potential of novel biosorbent candidates carboxyethyl chitosan (CEC) hydrogel and cryogel of carboxyethyl chitosan cross-linked with diglycidyl ether of butanediol-1,4 (10:1) (DEB-CEC) in removal of Allura Red dye from water.

2. Materials and methods

2.1. Gel preparation

Chitosan (degree of acetylation 16%, molecular weight 500 kDa) by Orison Chemicals Limited, China was used for CEC-based gels production.

2.1.1. CEC hydrogel preparation

CEC hydrogel preparation was carried out according to the procedure discussed previously [48]. In brief, a mixture of 1.65 g (0.01 mol) of chitosan and 1.35 ml (0.02 mol) of acrylic acid was prepared in 5.5 ml of water and kept at room temperature until gelation, followed by heating at 70 °C for 12 h. The resulting hydrogel was washed to neutral reaction and dried at the ambient temperature until constant weight.

2.1.2. DEB-CEC cryogel preparation

DEB-CEC cryogel was obtained by cross-linking of carboxyethyl chitosan obtained according to the previous procedure with diglycidyl ether of butanediol-1,4 at the "polymer:ether" molar ratio of 10:1, temperature –19 °C and pH 4 for 10 days.

The comprehensive scheme of the chitosan carboxyethylation and further cross-linking reaction is presented in Figure 3.

2.2. Gel characterization

2.2.1. FT-IR spectroscopy

The Fourier-transform infrared spectroscopy (FT-IR) was carried out using the spectrometer "Spectrum One" by Perkin Elmer (USA). The measurement was performed in triplicate.

2.2.2. Scanning electron microscopy

Scanning electron microscopy (SEM) was performed with a Zeiss EVO50 microscope (Germany) after metallization of the samples with a cuprum layer 20 nm thick using a JEOL JFC-1600 auto fine coater (Japan) at a pressure of no more than 8 Pa for 40 seconds.

2.2.3. Swelling capacity

The ability of samples to swell was determined using the gravimetric approach presented in various sources [49] and well recognized for biopolymer compositions. Before the test, the gel samples were dried to the constant mass, designated as W_d. Afterwards, the samples were immersed in 10 ml of distilled water at a temperature of 25 °C and kept for 30 min. Then the samples were retrieved, followed by, removing the excess medium on the surface with tissue paper and recording the weight (W_w).

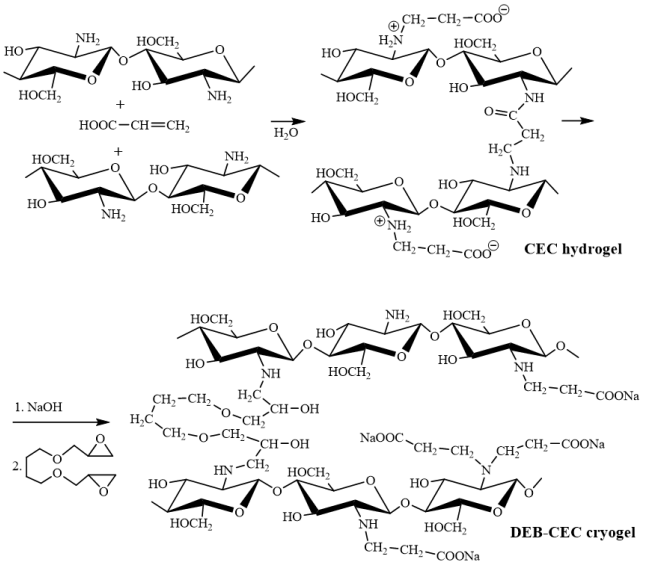

Figure 3 Scheme of the chitosan carboxyethylation and further cross-linking reaction with diglycidyl ether of butanediol-1,4.

 DOI: 10.15826/chimtech.2024.11.4.15

The swelling (S) in percent was calculated applying the following equation (1):

$$S\ (\%) = \frac{W_w - W_d}{W_d} \cdot 100\ \%. \quad (1)$$

2.2.4. Porosity

The porosity was measured by the liquid displacement method described in [50]. In the present study we chose ethanol as the displacement fluid; hence, it penetrates the sample without swelling or disrupting the structure. In brief, the dried sample of a mass recorded as W_d was immersed in ethanol under vacuum for 30 min, and the weight of the sample in ethanol was recorded as W_l. Next, the sample was removed and the liquid on its surface was removed with filter paper. The weight of the wet sample was designated W_w. The porosity (ε) was calculated according to equation (2):

$$\varepsilon\ (\%) = \frac{(W_w - W_d)}{(W_w - W_l)} \cdot 100\ \%. \quad (2)$$

2.2.5. Deacetylation degree

Deacetylation degree was evaluated via proton nuclear magnetic resonance spectroscopy (^{1}H NMR) using AVANCE 500, Bruker BioSpin (USA). The sample preparation was made through the treatment of gels with an aqueous solution of sodium hydroxide in order to destroy the cross-links and solubilize them, further recording the ^{1}H NMR spectrum.

2.3. Adsorption experiment

The experiment was performed using a stock solution of Allura Red AC (E129) prepared at 25 °C and neutral pH with a concentration of 5000 mg/L. The following concentrations were used to determine gel absorption kinetics: 100 mg/l (50 times dilution), 200 mg/l (25 times dilution), 300 mg/l (16.7 times dilution), 500 mg/l (10 times dilution), 600 mg/l (8.3 times dilution). 1 ml of each solution was added to Eppendorf vial containing the samples (0.05 g of gel each); then the measurements were made using a spectrophotometer Biobase BK-EL10C (China) after 10, 20, 40, 60, 120, 180 min at a λ = 450 nm. To do this, 100 µl of samples from experimental tubes were transferred into a 96-well plate compensating the sample volume with distilled water; water was used as a negative control, and a solution of intact dyes (0.5 mg/ml) was used as a positive control. The measurements were performed in triplicate. The following calibration curve was used to determine the concentration (Figure 4).

2.4. Adsorption kinetics study

The adsorption study was performed using three models, assessing the best fit of the experimental data with each of them. The presented models are widely applied to describe the adsorption of substances, including dyes, from wastewater using various biopolymers [30]:

- Pseudo-first order kinetic model (PFOM);
- Pseudo-second order kinetic model (PSOM);
- Intraparticle interaction model (IDM).

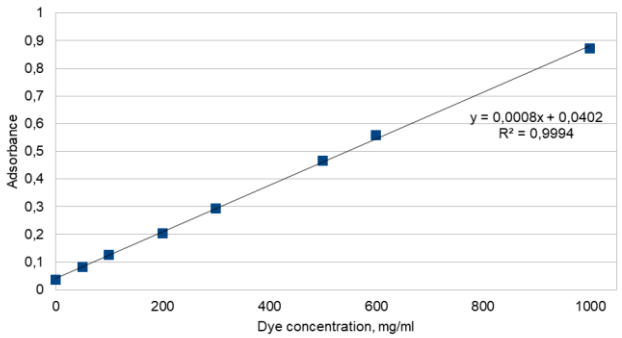

Figure 4 Calibration curve for E129 absorbance at λ = 450 nm.

The PFOM and PSOM were initially proposed to evaluate the homogeneous chemical reactions. Later on, these models were applied to heterogeneous systems including the effects of diffusion mechanisms within rate parameters.

2.4.1. Pseudo-first order kinetic model

Adsorption was initially described as a first-order reaction using a model proposed in 1898 by Lagergren, based on the adsorption of substances from solution onto the surface of coal. According to common opinion, it is the earliest model of kinetics. To distinguish kinetic equations based on adsorption capacity from equations and taking into account the concentration of adsorbate in solution, it is customary to denote these equations by the term “pseudo-first order”. The description of the kinetics within the framework of this model can be presented taking into account the occurrence of adsorption of sorbate molecules (M) on adsorption centers (A), equation (3):

$$A + M \underset{k_2}{\overset{k_1}{\rightleftarrows}} AM, \quad (3)$$

where A are the active centers on the surface of the sorbent, M is the sorbent in solution and AM is the sorbate associated with the active center; k_1 and k_2 are the rate constants of adsorption and desorption, respectively.

The adsorption from liquid medium can be described by the equation (4):

$$\frac{d\bar{q}}{dt} = k_{p1}\,(\bar{q}_e - \bar{q}_t), \quad (4)$$

where q_e and q_t are the amount of sorbed substance at equilibrium and at time t, respectively (mmol/g); k_{p1} – pseudo-first order rate constant (min^{-1}).

When integrating equation (4) with boundary and initial conditions q_t = 0 and $q_t = Q_t$ for t = 0 and t, the expression takes the form of equation (5) [40]:

$$\lg\,(Q_e - Q_t) = \lg\,(Q_e) - \frac{k_1}{2.303}t. \quad (5)$$

2.4.2. Pseudo-second order kinetic model

In 1998, Ho and Mackay presented a description of the kinetic process of adsorption of divalent metal ions by peat. Ion retention occurs due to the formation of a chemical bond

 DOI: 10.15826/chimtech.2024.11.4.15

with the polar carbonyl, carboxyl and alcohol functional groups of peat. The reaction is described by the equation (6):

$$2A^- + M^{2+} \Leftrightarrow A_2M. \quad (6)$$

The main assumption in this model is the use of the above equation, taking into account that adsorption is described by a second-order kinetics equation, and the limiting stage is adsorption with electrostatic interactions of functional groups of peat with metal ions. The adsorption isotherm is described by the Langmuir equation, the integral form of which for the dependence of the amount of adsorbed substance Q_t on time t has the form of equation (7):

$$Q_t = \frac{t}{\frac{1}{k_2 \cdot Q_e^2} + \frac{1}{Q_e}}, \quad (7)$$

where k_2 is the pseudo-second order sorption rate constant (g·(mmol·min)$^{-1}$); t – time (min).

Equation 7 does not require determination of the effective parameter Q_e, as in the pseudo-first order kinetics model. The applicability of the pseudo-second-order kinetics model for describing the sorption process is often demonstrated by the linearity of the dependence in the t/Q_t versus t coordinates. Using the tangent of the angle of inclination and the free term of the straight line, Q_e and k_2 can be calculated [52].

2.4.3. Intraparticle diffusion model

The kinetic results were also analyzed by the IDM to explain the adsorption behavior of E129 on both polymer systems and to understand the rate determining step. The dye adsorption may pass generally via liquid phase mass transport rate or through the intraparticle mass transport rate. The rate-limiting step may be as the boundary layer (film) so the intraparticle diffusion (pore) of the solute on the adsorbent surface from the bulk of the solution. In diffusion studies, the rate is generally expressed in terms of the square root of time. According to the IDM proposed by Weber and Morris [53], the time dependence can be determined from equation (8):

$$q_t = k_i\sqrt{t} + C \quad . \quad (8)$$

where q_t is the amount of solute on the surface of the sorbent at time t (mg/g), k_i is the rate constant of the intraparticle diffusion model (mg/g min$^{1/2}$), t is the time and C is the intercept (mg/g). The k_i values can be determined from the slopes of plots q_t versus $t^{1/2}$.

2.5. Isotherm analysis

Understanding the adsorption equilibrium is the key for evaluating the applicability of adsorption processes. The adsorption isotherms describe how solutes interact with adsorbent and are vital for optimizing the adsorption process conditions in regard to each polymer [54]. The batch adsorption experiment was done to obtain the adsorption curve. In brief, various solutions of Allura Red dye were prepared at 25 °C and neutral pH within a concentration of 100, 150, 200, 250, 300, 350, 400, 450, 500, 550 and 600 mg/L. 1 ml of each solution was added to Eppendorf vials each containing 0.05 g of gel samples; the measurements were made using the spectrophotometer Biobase BK-EL10C (China) after 180 min at a λ = 450 nm in triplicate. The resulting concentration was recalculated using the calibration curve obtained previously for the adsorption kinetic study (Figure 3). Various equilibrium isotherm equations were applied to describe the experimental sorption data obtained in this study, such as Freundlich, Langmuir and Temkin isotherms.

Langmuir isotherm model is the most known adsorption isotherm that is extensively used for the adsorption from liquid solutions. This model applies to the adsorption process onto a surface with a finite number of similar adsorption sites. The linearized form of Langmuir model is represented by equation (9) [55]:

$$\frac{C_e}{q_e} = \frac{1}{K_L} - \frac{a_L}{K_L} C_e \ , \quad (9)$$

where C_e (mg/L) and q_e (mg/g) are the liquid phase concentration and solid phase concentration of solute at equilibrium respectively. K_L (L/g) and a_L (L/mg) are the Langmuir isotherm constants. The constants K_L and a_L can be calculated based on the intercept ($1/K_L$) and the slope (a_L/K_L) of the linear plot of C_e/q_e versus C_e. The maximum adsorption capacity of the polymer, q_{max}, is defined as K_L/a_L.

The essential characteristic of Langmuir isotherm can be represented within the dimensionless constant (R_L), a so-called separation factor, and is given as equation (10):

$$R_L = \frac{1}{1 + a_L C_0}, \quad (10)$$

where C_o is the initial concentration of dye (mg/L) and a_L is the Langmuir constant related to the adsorption energy (L/mg). Depending on the value of R_L, the adsorption process can be an unfavorable process (R_L>1), linear (R_L = 1), favorable (R_L between 0 and 1) or irreversible (R_L = 0) [61]. Another isotherm model proposed by Freundlich considers that the adsorption occurs on heterogeneous surfaces and multilayer sorption. This model suggests that adsorption energy exponentially decreases upon the adsorbent sorption centers completion, and it is employed to describe heterogeneous systems via building the linear form of the Freundlich expression, equation (11) [57]:

$$\ln q_e = \ln K_F + \frac{1}{nF} \ln C_e, \quad (11)$$

where q_e is the amount of solute (dye) adsorbed at equilibrium time (mg/g), C_e is the equilibrium concentration solute in solution (mg/L), K_F is the Freundlich constant (L/g) related to the energy of bonding and $1/nF$ is the heterogeneity factor. The $1/nF$ and K_F values are generated as the slope and intercept of plots lnq_e versus lnC_e, respectively.

Temkin model comprises the effects of indirect solute/adsorbent interactions on adsorption isotherms and suggests that the heat of adsorption of all molecules in the

 DOI: 10.15826/chimtech.2024.11.4.15

layer decreases linearly with coverage because of their interactions [62]. The adsorption is characterized by the uniform distribution of bond energies until the bond energy reaches its maximum. The linear form of Temkin equation is presented as equation (12) [58]:

$$q_e = \frac{RT}{bT}\ln a_T + \frac{RT}{bT}\ln C_e, \quad (12)$$

where T is the absolute temperature in Kelvin, R is the universal gas constant (8.314 J/mol K), a_T is the constant of Temkin isotherm (L/g) and bT is the Temkin constant, related to the heat of adsorption (kJ/mol). The Temkin constants a_T and β (RT/bT) are calculated from the slope and intercept of the linear plot of q_e versus lnC_e.

2.6. Statistical analysis

Statistical analysis was performed using IBM SPSS Statistics software (version 25.0). For all collected kinetics data we built linear regression models. The presented model data includes linear regression coefficient value R^2, root mean square error (RMSE) and significance level p-value. The models were considered reliable if both $R^2 > 0.80$ and a significance level was less than the designated alpha value. In the text of the manuscript, the significance levels are indicated either as absolute values or (for exponential values) as $p < 0.0001$.

3. Results and Discussion

Compared with chitosan, which is widely used for various purposes, CEC has a number of advantages, including solubility over the entire pH range [48], reduced toxicity [59], safety for biomedical applications [60], mechanical controllability [61], drug and bacterial carrier [63, 64], wound healing [65] and tissue engineering [66]. It is now also agreed upon that cryotechnology allows producing a specific type of hydrogels called cryogels with porous structure, which have wide surface area, attractive for adsorption application.

3.1. Gel characterization

Except for external conditions, the adsorption process highly depends on different physical-chemical characteristics of adsorbent, the type of polymer prepared, and its chemical structure and functional groups. In this regard, we characterized the polymer systems as follows.

3.1.1. FT-IR spectroscopy

The FT-IR spectroscopy data show (Figure 5) that, for CEC aside from the main IR-bands at 3291 (O–H, N–H), 2856 (C–H), 1314 (O–H), 1062, 1022 (C–N, C–O) cm^{-1} typical of chitosan, new bands appear at 2918 (C–H), 1775, 1734 (O=C–OH), 1561 (O=C–O–) and 1419 (C–H) cm^{-1}, which indicate successful functionalization of chitosan with 2-carboxyethyl groups. Moreover, the more intense absorption band at 1561 cm^{-1} compared to the bands at 1775 and 1734 cm^{-1} indicates the predominant zwitterionic form of the polymer.

The lack of solubility of CEC enables the formation of a hydrogel due to the crosslinking by amide bonds that are formed during the addition of chitosan to acrylic acid [48]. The small amount of amide bonds is confirmed by a new absorption band at 1658 (O=C amide) cm^{-1}. Treatment of CEC with an aqueous alkali solution leads to the destruction of these bonds and polymer becomes soluble. Further treatment of the polymer with diglycidyl ether of butanediol-1,4 forms a new type of cross-linking with ether bonds.

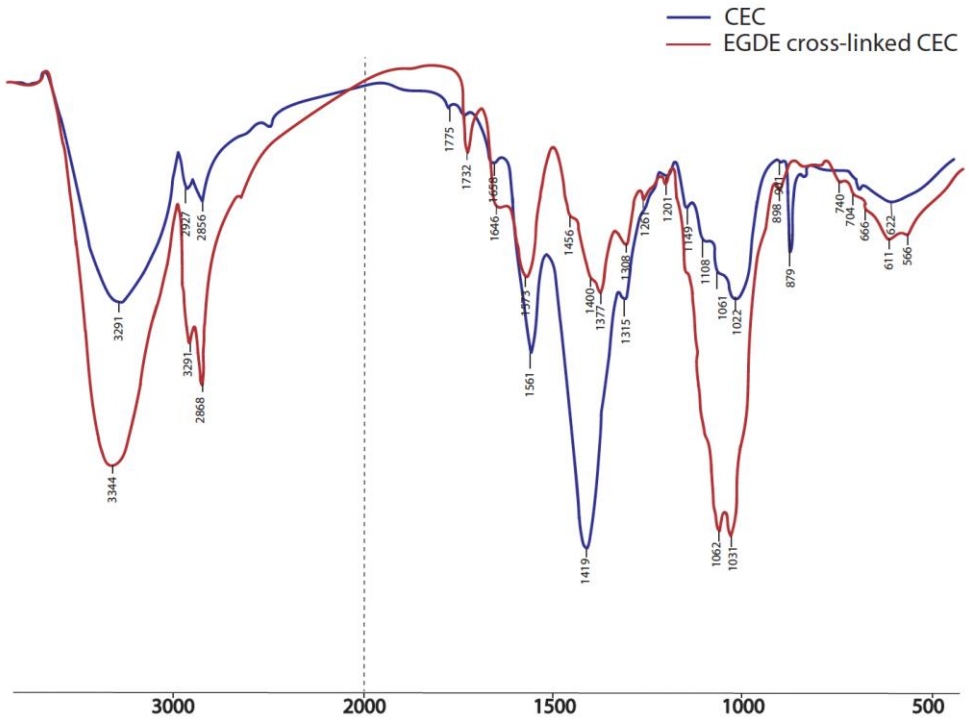

Figure 5 FT-IR spectra for CEC (down) and for DEB-CEC (up).

 DOI: 10.15826/chimtech.2024.11.4.15

For this reason, the spectrum of DEB-CEC does not change fundamentally, except for the disappearance of the absorption band at 1658 cm^{-1} – a band appears at 1649 cm^{-1}, which corresponds to the amide bond in the acetyl group, and changes in the relative intensity of the absorption bands.

3.1.2. Scanning electron microscopy

The CEC-based structures were studied in both dried and swollen states. The results presented in Figure 6 showed that both samples have heterogeneous pore structure in the dried state. However, we detected the hole formation inside of the already existing pores in the swollen CEC hydrogel, which happened due to swelling increasing the distance between CEC layers and can increase the effective surface. On the contrary, DEB-CEC cryogel showed excellent pore formation resulting in regular structure with the pore size from 18 up to 50 nm, which comes in agreement with current opinion on the cross-linked cryogels [67, 68]. In this regard, DEB-CEC cryogel can demonstrate good adsorption properties towards different objects.

3.2. Gel characterization

In the context of the adsorption evaluation, we consider swelling and porosity as key parameters of CEC-based structures, which influence the adsorption, hence they determine the surface area available for contact with solution. Also, due to the possible binding of the ARD by free amino-group, their content is also important for adsorption evaluation. As a result, the swelling and porosity values were 244.97% and 54.50%, respectively, for CEC hydrogel and 429.91% and 148.00% for DEB-CEC. So far, structure characteristics of the samples demonstrated that the adsorption capacity of DEB cross-linked CEC should be higher compared to CEC hydrogel. Our next step was to check this hypothesis.

3.3. Adsorption kinetics

Adsorption depends on several factors, such as surface area, adsorbent and adsorbate properties, their mass ratio, the temperature of the system, the nature of the solvent, and the pH [69]. The adsorption data for the removal of E129 versus contact time at different concentrations of dye (from 99.4048 to 627.2619 mg/L) for the polymers are presented as a function of q_t versus time, measured in minutes, presented in Figure 7.

Figure 7 demonstrates that the adsorption of dye on the polymer achieved saturation. This means that the amount of adsorbed dye inside the polymer was in a dynamic equilibrium with the amount of dye released after 120 min. At this point the amount of dye removed by adsorbent at a certain time indicates the maximum adsorption capacity of each polymer under investigated conditions. According to data the adsorption gradually increased during the initial period between the dye and polymer due to swelling. At the next step the adsorption was continuous until the equilibrium was reached.

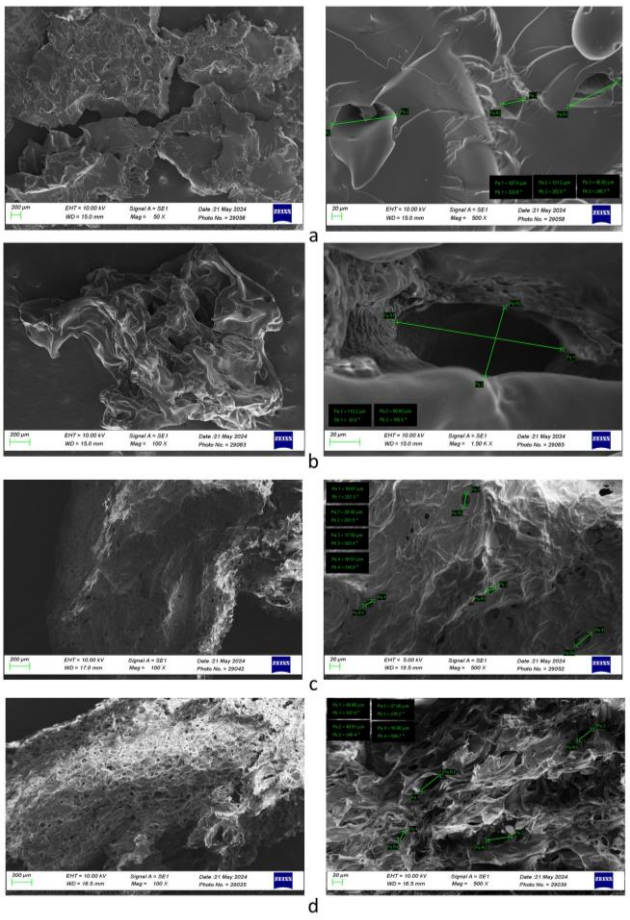

Figure 6 SEM micrographs of CEC and DEB-CEC gels in different states: a) CEC hydrogel dried, b) CEC hydrogel swollen, c) DEB-CEC cryogel dried, d) DEB-CEC cryogel swollen.

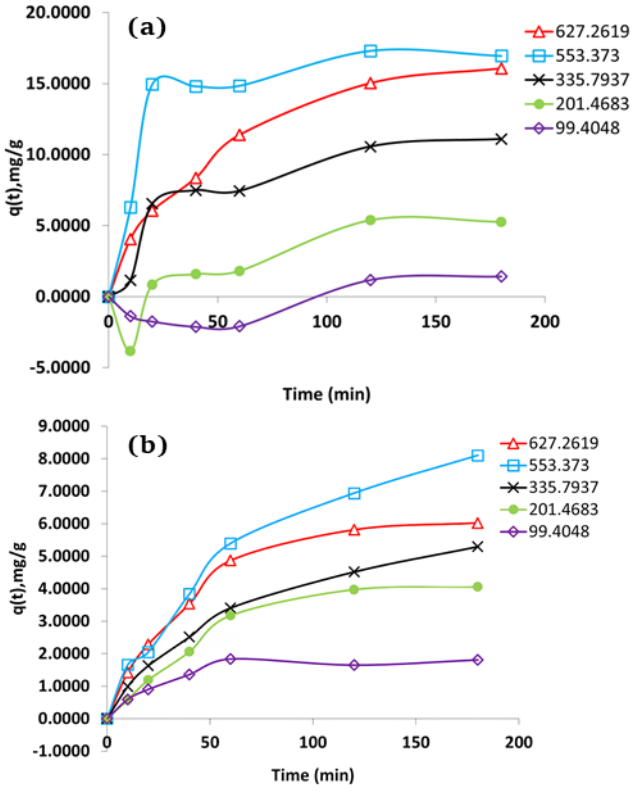

Figure 7 Adsorption curves as a function of dye concentration in mg/L for a) CEC hydrogel, b) DEB-CEC cryogel.

 DOI: 10.15826/chimtech.2024.11.4.15

All curves were asymptotic after approximately 120 min of contact time. In this regard the adsorption process could be considered moderate. However, upon the concentration growth, both biopolymers tend to adsorb higher amounts of the dye, confirming the strong interaction between the dye and adsorbent.

Next, to test the experimental data obtained in the adsorption of Allura Red and carboxyethyl chitosan-derived polymers, the pseudo-first-order, pseudo-second-order and the intraparticle diffusion models were employed with the purpose to determine the different mechanisms implicated in the adsorption process, such as adsorption surface, mass transfer or intraparticle diffusion.

3.3.1. Pseudo-first order kinetic model

Using the resulting equation 6, it is possible to determine the adsorption rate (k_1) graphically, expressing the dependence of $\log(q_e - q_t)$ on t (Figure 8), which allows one to calculate the adsorption rate in the form of a constant k_1, as well as analyze experimental data within the framework of the pseudo-first order kinetics model. Description of kinetics within the framework of this model allows us to consider the sorbate-sorbent or sorbate-sorbate interactions.

The experimental data fits to the pseudo-first-order plots, which is shown in Figure 8, and the corresponding parameters and linear regression coefficient R^2 values are given in Table 2.

The linearity of the model ($\log(q_e - q_t)$ versus t) was plotted for 120 min of contact for both polymers. The regression coefficient values for CEC ranged from 0.364 to 0.996, while for DEB-CEC the correlation coefficient varied from 0.954 and 0.993.

Theoretical values of q_e were compared with the experimental data. Taking into account the sufficient difference between the q_{eexp} and q_{ecal}, we considered the results obtained for CEC demonstrated poor fit to the PFOM model, while for DEB-CEC the fit was acceptable. Because of these results, it was appropriate to study the pseudo-second-order model with the experimental data obtained.

3.3.2. Pseudo-second order kinetic model

In the case of the data obtained, the pseudo-second order adsorption graphs look as follows (Figure 9). The experimental data fits to the pseudo-second-order plots better for DEB-CEC, which is shown in Figure 9 and the corresponding parameters and R^2 in Table 3. The linearity of the model t/q_t versus t was plotted for 180 min of contact and the R^2 values for CEC ranged from 0.364 to 0.996. At the same time for DEB-CEC the linear regression coefficient R^2 values were from 0.954 and 0.993.

Theoretical values of q_e are similar to those obtained during the adsorption experiment, which confirms better fit of the data to PSOM. However, there is a small difference between q_{eexp} and q_{ecal}, which pushed us to evaluate the data using the intraparticle diffusion kinetic model.

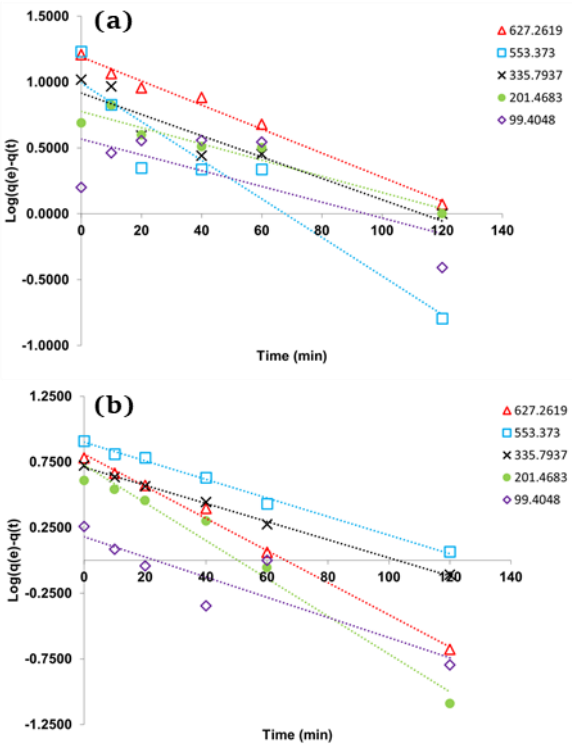

Figure 8 Pseudo-first order adsorption plots as a function of dye concentration in mg/ml for a) CEC hydrogel, b) DEB-CEC cryogel.

Table 2 The kinetic parameters of the PFOM for the adsorption of Allura Red onto CEC and DEB-CEC polymers.

Name	C_o (mg/g)	$q_{e\,exp}$ (mg/g)	PFOM parameters				
			k_1 (min^{-1})	$q_{e\,cal}$ (mg/g)	R^2	RMSE	*p*-value
CEC	627.262	16.140	-0.010	6.701	0.990	0.313	<0.0001
	553.373	17.181	-0.020	21.883	0.996	0.221	<0.0001
	335.794	10.871	-0.015	15.008	0.759	2.141	<0.0001
	201.468	5.140	-0.010	8.083	0.364	11.135	0.008
	99.405	1.519	-0.007	2.798	0.819	26.993	<0.0001
DEB-CEC	627.262	6.137	-0.012	8.932	0.993	0.698	<0.0001
	553.373	8.153	-0.007	14.624	0.961	1.109	<0.0001
	335.794	5.390	-0.007	9.860	0.993	0.720	<0.0001
	201.468	4.006	-0.015	5.509	0.954	2.390	<0.0001
	99.405	1.898	-0.012	2.808	0.979	4.294	<0.0001

 DOI: 10.15826/chimtech.2024.11.4.15

Table 3 The kinetic parameters of the PSOM for the adsorption of Allura Red onto CEC and DEB-CEC polymers.

Name	C_o (mg/g)	$q_{e\ exp}$ (mg/g)	PSOM parameters				
			k_1 (min^{-1})	$q_{e\ cal}$ (mg/g)	R^2	RMSE	*p*-value
CEC	627.262	16.140	−0.010	6.701	0.989	0.042	<0.0001
	553.373	17.181	−0.020	21.883	0.846	0.228	<0.0001
	335.794	10.871	−0.015	15.008	0.919	0.134	<0.0001
	201.468	5.140	−0.010	8.083	0.668	0.105	<0.0001
	99.405	1.519	−0.007	2.798	0.488	0.292	0.001
DEB-CEC	627.262	6.137	−0.012	8.932	0.994	0.039	<0.0001
	553.373	8.153	−0.007	14.624	0.992	0.027	<0.0001
	335.794	5.390	−0.007	9.860	0.995	0.019	<0.0001
	201.468	4.006	−0.015	5.509	0.962	0.098	<0.0001
	99.405	1.898	−0.012	2.808	0.728	0.204	<0.0001

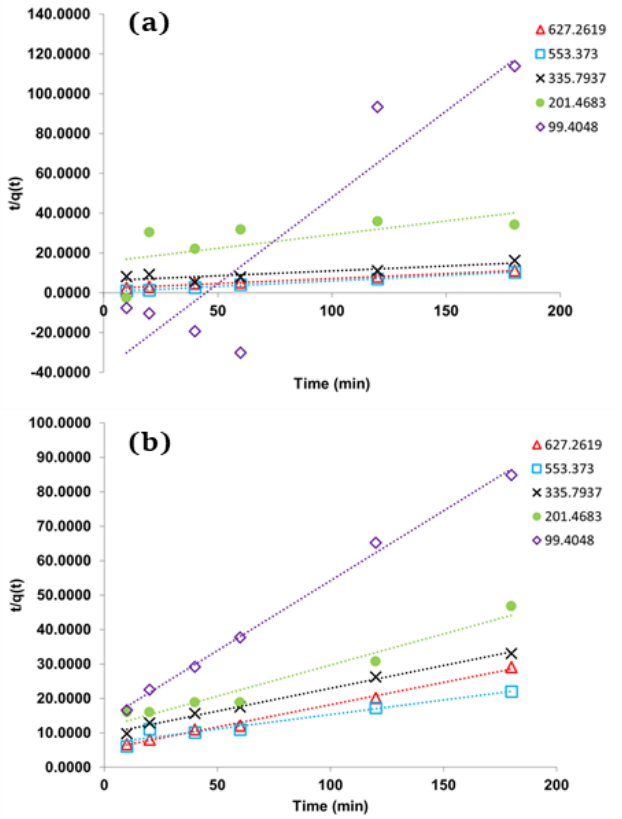

Figure 9 Pseudo-second order adsorption plots as a function of dye concentration in mg/ml for a) CEC hydrogel, b) DEB-CEC cryogel.

3.3.3. Intraparticle diffusion model

Generally, adsorption represents a process with different stages that implicates a transport of solute molecules from the solution and further diffusion thereof onto the adsorbent surface. Taking into account the polymeric structure of the adsorbent, we considered that the intraparticle diffusion influences the adsorption process. We studied this effect through plotting the amount of Allura Red adsorbed versus the square root of time, which represents the intraparticle diffusion model (Figure 10). The kinetics results obtained can be used to investigate whether the intraparticle diffusion is the limiting step in the adsorption of the dye inside the polymer matrix.

The intraparticle diffusion constant (k_i) values are represented in Table 4. These values increased along with concentrations of Allura Red. DEB cross-linked CEC showed better linear regression values compared to CEC, ranging from 0.820 to 0.988 and from 0.603 to 0.968, respectively.

It can be seen that the results obtained for each curve do not cross the origin, which allows one to conclude that the IDM is not the rate-limiting step besides its involvement into the adsorption process. This means that different processes control adsorption rate and the adsorption in the present case passes through different stages.

The *C* (intercept) values of Table 4 demonstrates how thick the boundary layer is. A higher intercept correlates with the higher effect of the layer. In this experiment, the C (intercept) values increased for both polymeric systems, and CEC has a higher effect of the boundary layer compared to DEB-CEC polymer.

Summarizing the adsorption kinetics data we concluded that the adsorption rate for DEB-CEC is better represented by PSOM with a rapid growth at the initial adsorption step with further saturation, while for CEC hydrogel the adsorption process is rather complex with a closest fit to PFOM with relatively low regression coefficient meaning.

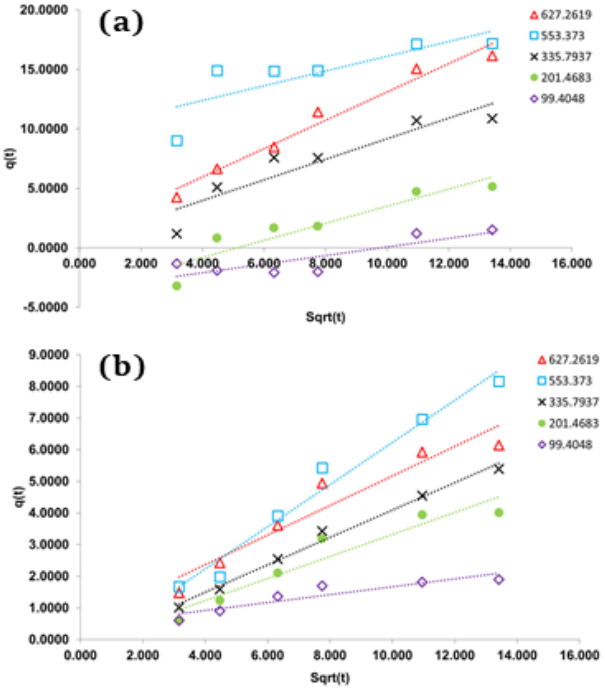

Figure 10 Intraparticle diffusion model plots as a function of dye concentration in mg/ml for a) CEC hydrogel, b) DEB-CEC cryogel.

 DOI: 10.15826/chimtech.2024.11.4.15

Table 4 The kinetic parameters of the IDM for the adsorption of Allura Red onto CEC and DEB-CEC polymers.

Name	C_o (mg/g)	$q_{e\,exp}$ (mg/g)	IDM parameters					
			k_i (g/mg min$^{1/2}$)	$q_{e\,cal}$ (mg/g)	R^2	RMSE	*p*-value	*C* (intercept, mg/g)
CEC	627.262	16.140	1.190	17.150	0.968	0.814	<0.0001	1.186
	553.373	17.181	0.619	18.209	0.603	1.899	<0.0001	9.905
	335.794	10.871	0.867	12.137	0.805	1.612	<0.0001	0.510
	201.468	5.140	0.718	5.942	0.821	1.266	<0.0001	−3.693
	99.405	1.519	0.361	1.313	0.709	0.875	<0.0001	−3.532
DEB-CEC	627.262	6.137	0.636	5.198	0.918	0.528	<0.0001	−3.331
	553.373	8.153	0.508	3.706	0.970	0.427	<0.0001	−3.115
	335.794	5.390	0.803	7.560	0.988	0.175	<0.0001	−3.214
	201.468	4.003	0.853	8.569	0.910	0.414	<0.0001	−2.880
	99.405	1.902	1.876	21.8383	0.820	0.221	<0.0001	−3.335

This observation can be described by the structural difference between the biopolymers because of cross-linking. We suppose that the key adsorption mechanism of Allura Red dye by CEC involves hydrogen bond formation between an increased number of carboxyethyl groups which are further partially blocked by the cross-linking resulting in q_e decrease.

3.4. Adsorption equilibrium

The experimental data of adsorption equilibrium between Allura Red and CEC as well as DEB cross-linked CEC polymers were studied applying Langmuir, Freundlich and Temkin isotherm models within plots and constants presented at Figure 11 and Table 5, respectively.

The Freundlich isotherm is presented as the plot of lnq_e versus lnC_e. The linear are given for both polymers is presented at Figure 10.

The key parameters obtained for CEC hydrogel and DEB cross-linked CEC, respectively, are as follows: K_F = 56.371 L/g and 15.529 L/g, n_F = 1.480 and 2.445, R^2 = 0.964 and 0.853. The adsorption process is considered favorable when the value of n_F fits into the range between 1–10, which is confirmed for both biopolymers. Temkin isotherm obtained as the plot of q_e versus lnC_e (Figure 11). The meaning of a_t, b_t parameters were calculated as 161.500 and 535.483 for CEC hydrogel with R^2 = 0.932 and 347.501 and 1391.660 for DEB-CEC with R^2 = 0.816.

Langmuir isotherm was obtained as the plot of C_e/q_e versus C_e. For both polymers the a_L/K_L can be determined as the slope, the intercept is a $1/K_L$ and K_L/a_L is the parameter q_{max} which is the maximum adsorption capacity of each polymer (mg/g).

The q_{max} value obtained for CEC hydrogel was 22.523 mg/g and for DEB-CEC the value was 10.482 mg/g, which are rather close to experimental q_e of 18.209 mg/g and 9.560 mg/g, respectively. Comparing the theoretical and experimental values demonstrates that the saturation was achieved for both biopolymers. Transferring the obtained meanings into molar adsorption we received the values of 45.4 μmol/g for CEC and 21.1 μmol/g for DEB-CEC, indicating that CEC demonstrated better adsorption capacity towards Allura Red compared to DEB-CEC. Within the analysis of the obtained data one can suggest low adsorption capacity of CEC-based biopolymers. However, it should be mentioned that the adsorption experiment was performed in unfavorable conditions of neutral pH, and the results are less than the capacity of an activated carbon (146.75 μmol/g) [23].

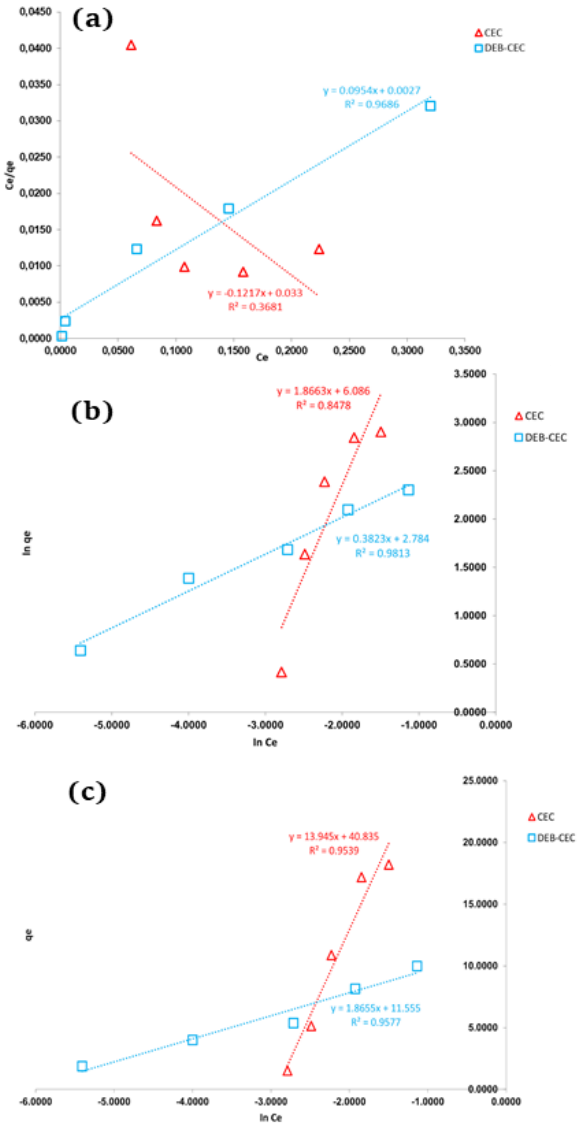

Figure 11 Adsorption isotherms plots for a) Langmuir model, b) Freundlich model, c) Temkin model.

 DOI: 10.15826/chimtech.2024.11.4.15

Table 5 Adsorption constants for Langmuir, Freundlich and Temkin models.

Isotherm	Parameter	CEC	DEB-CEC
Langmuir	K_L	14.323	35.333
	q_{max}	22.523	10.482
	R^2	0.675	0.967
	RMSE	0.001	0.002
	p-value	0.006	<0.0001
Freundlich	K_F	56.371	15.529
	n_F	1.480	2.445
	R^2	0.964	0.853
	RMSE	0.213	0.435
	p-value	<0.0001	<0.0001
Temkin	a_t	161.500	347.501
	b_t	535.483	1391.660
	R^2	0.932	0.816
	RMSE	0.296	0.487
	p-value	<0.0001	<0.0001

Adsorption capacity of chitosan at the same pH was estimated as 131.74 μmol/g [31]. So far, we can conclude that the amino-group interaction with dye is crucial for Allura Red adsorption, hence the carboxyalkylation led to adsorption capacity decrease. Moreover, we suppose that the hydrogen-bonding mechanism is also involved in the Allura Red adsorption process because of further decrease of qmax for cross-linked CEC. Based on the calculated parameters, we applied the experimental data of q_e obtained within the batch adsorption experiment to the corresponding adsorption isotherms (Figure 12) proving that the Allura Red dye adsorption fits best Temkin isotherm and that the dye forms a monolayer involving the intermolecular interaction between biopolymers and the adsorbate.

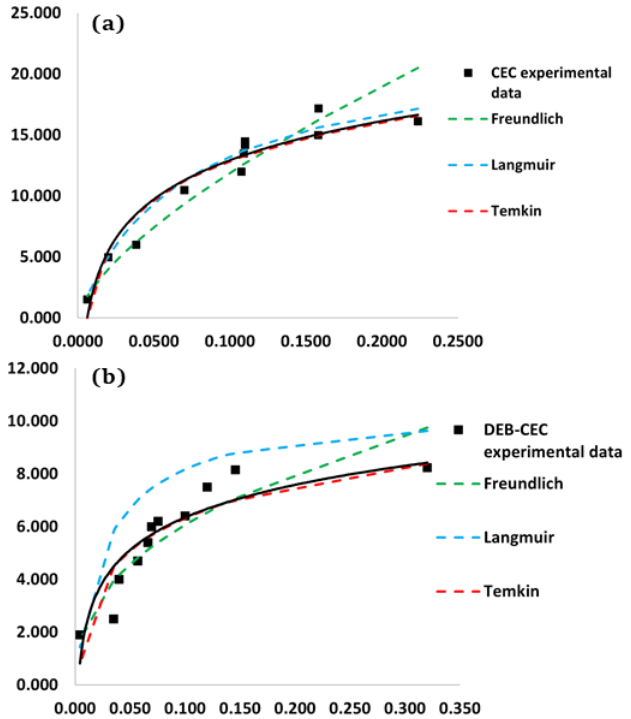

Figure 12 Adsorption isotherms for a) CEC, b) DEB-CEC.

4. Limitation

The adsorption process of Allura Red dye on carboxyethyl chitosan derivatives was performed in the unfavorable conditions, which limited the adsorption rate. We believe that, further investigation is required to specify the optimal adsorption conditions including pH, temperature, particle size and functionalization degree of carboxyethyl chitosan.

5. Conclusions

New carboxyethyl chitosan based adsorbents were prepared by "green" carboxyalkylation approach and further cross-linking with butanediol-1,4 diglycidyl ether. The adsorbents were characterized with FTIR, SEM, estimation of porosity and swelling capacity and further successfully applied for removal of Allura Red dye from aqueous solutions at neutral pH at 25 °C varying initial dye concentrations from 99.4 up to 627.3 mg/L. Adsorption isotherms and kinetic models were used to investigate the interaction mechanism between biosorbents and Allura Red.

Adsorption data best fitted with Temkin isotherm for both polymers; q_{max} was 22.523 mg/g (45.4 μmol/g) for CEC and 10.482 mg/g (21.1 μmol/g) for DEB-CEC, while the kinetics was different. The adsorption rate for DEB-CEC is better represented by PSOM with a rapid growth at the initial adsorption step with further saturation, while for CEC hydrogel the adsorption process is rather complex with a closest fit to PFOM. The Temkin model was found to be the best to describe the adsorption isotherm of Allura Red dye.

The observed decrease of the adsorption capacity compared to chitosan was correlated with its carboxyalkyl derivatization and further cross-linking, affecting the interaction of amino-groups with Allura Red and hydrogen bonding formation, respectively. So far, the present study demonstrated that CEC and DEB-CEC polymers can be applied as biodegradable and eco-friendly biosorbents for Allura Red dye removal from aqueous solutions, and extra experiments are required to find the optimal conditions for Allura Red dye adsorption by biopolymers. This gives the opportunity to use these adsorbents in wastewater treatment to prevent environment pollution by azo-dyes.

• Supplementary materials

No supplementary materials are available.

• Funding

This research was supported by the "Priority-2030" program in Novosibirsk State Technical University (project no. SP-3 Zh-5).

• Acknowledgments

None.

 DOI: 10.15826/chimtech.2024.11.4.15

• Author contributions

Conceptualization: A.A.D. E.A.B.
Data curation: A.A.D., E.A.L.
Formal Analysis: A.G.S.
Funding acquisition: E.A.B.
Investigation: A.V.K., D.V.L., E.O.Z., A.V.P.
Methodology: E.A.B., A.V.K., P.I.D.
Project administration: E.A.B.
Supervision: E.A.L.
Visualization: P.I.D., E.A.L.
Writing – original draft: A.A.D., A.V.K.
Writing – review & editing: A.A.D., E.A.B., A.G.S., A.V.P., E.A.L.

• Conflict of interest

The authors declare no conflict of interest.

• Additional information

Author IDs:

Aleksandr A. Drannikov, Scopus ID 57210816225;
Elena A. Blinova, Scopus ID 57189237767;
Anastasya V. Korel, Scopus ID 23497454800;
Alexander G. Samokhin, Scopus ID 57200373388;
Polina I. Dubovskaya, Scopus ID 25627090600;
Ekaterina O. Zemlyakova, Scopus ID 57204198523;
Alexander V. Pestov, Scopus ID 11439505900;
Ekaterina A. Litvinova, Scopus ID 7005626124.

Websites:

Novosibirsk State Technical University, https://en.nstu.ru/.

I. Ya. Postovsky Institute of Organic Synthesis, UB RAS, https://www.iosuran.ru/page/about.

References

1. Pavithra KG, Kumar PS, Jaikumar V, Rajan PS. Removal of colorants from wastewater: A review on sources and treatment strategies. J Ind Eng Chem. 2019;75:1–19. doi:10.1016/j.jiec.2019.02.011
2. de Mejia EG, Zhang Q, Penta K, Eroglu A, Lila MA. The colors of Health: Chemistry, Bioactivity, and market Demand for colorful Foods and natural Food sources of Colorants. Annu Rev Food Sci Technol. 2020;11(1):145–182. doi:10.1146/annurev-food-032519-051729
3. Hocine H, Benettayeb A, Al-Farraj S, Ali Alkahtane A, Olivier J, Sillanpaa M. Turbidity removal from synthetic Bentonite suspension Using opuntia Ficus-indica (Cactus). Int Rev Civ Eng (IRECE). 2024;15(1):12. doi:10.15866/irece.v15i1.23223
4. Benkhaya S, El Harfi S, El Harfi A. Classifications, properties and applications of textile dyes: A review. Appl. J. Envir. Eng. Sci. 2017;3(3):311-20 doi:10.48422/IMIST.PRSM/ajees-v3i3.9681
5. Tkaczyk A, Mitrowska K, Posyniak A. Synthetic organic dyes as contaminants of the aquatic environment and their implications for ecosystems: A review. Sci Total Environ. 2020;717:137222. doi:10.1016/j.scitotenv.2020.137222
6. Thiam A, Sirés I, Garrido JA, Rodríguez RM, Brillas E. Decolorization and mineralization of allura Red AC aqueous solutions by electrochemical advanced oxidation processes. J Hazard Mater. 2015;290:34–42. doi:10.1016/j.jhazmat.2015.02.050
7. Oussadi K, Al-Farraj S, Benabdallah B, Benettayeb A, Haddou B, Sillanpaa M. Wool keratin as a novel, alternative, low-cost adsorbent rich in various –N and –S proteins for eliminating methylene blue from water. Biomass Convers Biorefinery. 2024:1-15. doi:10.1007/s13399-024-05851-4
8. Amar IA, Abdulqadir MA, Benettayeb A, Lal B, Shamsi SA, Hosseini-Bandegharaei A. Cerium-doped Calcium ferrite for malachite Green dye Removal and antibacterial Activities. Chem Afr. 2024;7(3):1423–41. doi:10.1007/s42250-023-00834-w
9. Hofseth LJ, Hebert JR, Murphy EA, Trauner E, Vikas A, Harris Q, Chumanevich AA. Allura Red AC is a xenobiotic. Is it also a carcinogen? Carcinogenesis. 2024 Oct 10;45(10):711-20. doi: 10.1093/carcin/bgae057
10. Renita AA, Gajaria TK, Sathish S, Kumar JA, Lakshmi DS, Kujawa J, Kujawski W. Progress and prospective of the industrial Development and applications of Eco-friendly Colorants: an Insight into environmental Impact and sustainability Issues. Foods. 2023;12(7):1521. doi:10.3390/foods12071521
11. Feketea G, Tsabouri S. Common food colorants and allergic reactions in children: Myth or reality? Food Chem. 2017 Sep 1;230:578-88. doi: 10.1016/j.foodchem.2017.03.043.
12. Silva MM, Reboredo FH, Lidon FC. Food colour Additives: A synoptical Overview on their Chemical Properties, applications in food Products, and health Side Effects. Foods. 2022;11(3):379. doi:10.3390/foods11030379
13. Benkhaya S, M'rabet S, El Harfi A. Classifications, properties, recent synthesis and applications of azo dyes. Heliyon. 2020;6(1):e03271. doi:10.1016/j.heliyon.2020.e03271
14. Rovina K, Siddiquee S, Shaarani SM. Extraction, analytical and advanced Methods for detection of allura Red AC (E129) in food and beverages Products. Front Microbiol. 2016;7. doi:10.3389/fmicb.2016.00798
15. Scientific opinion on the re-evaluation of allura Red AC (E 129) as a food additive. EFSA J. 2009;7(11):1327. doi:10.2903/j.efsa.2009.1327
16. Tsuda S. DNA damage Induced by red Food dyes Orally administered to pregnant and male Mice. Toxicol Sci. 2001;61(1):92–99. doi:10.1093/toxsci/61.1.92
17. Zhang Q, Chumanevich AA, Nguyen I, Chumanevich AA, Sartawi N, Hogan J, Khazan M, Harris Q, Massey B, Chatzistamou I, Buckhaults PJ, Banister CE, Wirth M, Hebert JR, Murphy EA, Hofseth LJ. The synthetic food dye, Red 40, causes DNA damage, causes colonic inflammation, and impacts the microbiome in mice. Toxicol Rep. 2023 Sep 6;11:221–32. doi: 10.1016/j.toxrep.2023.08.006
18. McCann D, Barrett A, Cooper A, Crumpler D, Dalen L, Grimshaw K, Kitchin E, Lok K, Porteous L, Prince E, Sonuga-Barke E, Warner JO, Stevenson J. Food additives and hyperactive behaviour in 3-year-old and 8/9-year-old children in the community: a randomised, double-blinded, placebo-controlled trial. Lancet. 2007;370(9598):1560–1567. doi:10.1016/s0140-6736(07)61306-3
19. Noorafshan A, Hashemi M, Karbalay-Doust S, Karimi F. High dose Allura Red, rather than the ADI dose, induces structural and behavioral changes in the medial prefrontal cortex of rats and taurine can protect it. Acta Histochem. 2018 Aug;120(6):586-94. doi: 10.1016/j.acthis.2018.07.004
20. Benkhaya S, M'rabet S, Lgaz H, El Bachiri A, El Harfi A. Dyes: Classification, Pollution, and environmental Effects. Sustain Text: Prod, Process, Manuf & Chem. 2022:1–50. doi:10.1007/978-981-16-5932-4_1
21. Ahmad A, Mohd-Setapar SH, Chuong CS, Khatoon A, Wani WA, Kumar R, Rafatullah M. Recent advances in new generation dye removal technologies: novel search for approaches to reprocess wastewater. RSC Adv. 2015;5(39):30801–30818. doi:10.1039/c4ra16959j

22. Mashkoor F, Nasar A, Inamuddin. Carbon nanotube-based adsorbents for the removal of dyes from waters: A review. Environ Chem Lett. 2020;18(3):605–629. doi:10.1007/s10311-020-00970-6
23. Alkahtani SA, Abu-Alrub SS, Mahmoud Am. Adsorption of food coloring allura red dye (e129) from aqueous solutions using activated carbon. Int J Food Allied Sci. 2017;3(1):10. doi:10.21620/ijfaas.2017110-26
24. Ullah R, Iftikhar F, Ajmal M, Shah A, Akhter M, Ullah H, Waseem A. Modified clays as an efficient Adsorbent for brilliant Green, ethyl Violet and allura Red Dyes: kinetic and thermodynamic Studies. Pol J Environ Stud. 2020;29(5):3831–3839. doi:10.15244/pjoes/112363
25. Saidobbozov S, Nurmanov S, Qodirov O, Parmanov A, Nuraliyev S, Berdimurodov E, Hosseini-Bandegharaei A, Nik WMNBW, Benettayeb A, Mubarak NM, Berdimuradov K. Extraction of indene from local pyrolysis oil and its usage for synthesis of a cationite. Chem Pap. 2024;78(15):8333–50. doi:10.1007/s11696-024-03671-4
26. Şenol ZM. Effective biosorption of allura red dye from aqueous solutions by the dried-lichen (pseudoevernia furfuracea) biomass. Int J Environ Anal Chem. 2022;102(16):4550–4564. doi:10.1080/03067319.2020.1785439
27. Ghosh S, Benettayeb A, Meskini M, Lal B, Al-Sharify ZT, Ajala OJ, Osagie C, Malloum A, Al-Najjar SZ, Onyeaka H, Bornman C, Ahmadi S, Igwegbe CA, Hosseini-Bandegharaei A. Advancing wastewater treatment with azolla filiculoides waste: a comprehensive review of adsorption applications. Environ Technol Rev. 2024;13(1):359–78. doi:10.1080/21622515.2024.2354126
28. Amela K, Hassen MA, Kerroum D. Isotherm and kinetics Study of biosorption of cationic Dye onto banana Peel. Energy Procedia. 2012;19:286–295. doi:10.1016/j.egypro.2012.05.208
29. Saha TK, Bishwas RK, Karmaker S, Islam Z. Adsorption characteristics of allura Red AC onto sawdust and hexadecylpyridinium Bromide-treated Sawdust in aqueous Solution. ACS Omega. 2020;5(22):13358–13374. doi:10.1021/acsomega.0c01493
30. Benettayeb A, Ahamadi S, Ghosh S, Malbenia John M, Mitchel CR, Haddou B. Natural adsorbents for the removal of emerging pollutants and its adsorption mechanisms. Sustain Technol Remediat Emerg Pollut Aqueous Environ. 2024:63–78. doi:10.1016/B978-0-443-18618-9.00013-9
31. Piccin JS, Dotto GL, Vieira MLG, Pinto LAA. Kinetics and mechanism of the food Dye FD&C red 40 adsorption onto Chitosan. J Chem & Eng Data. 2011;56(10):3759–3765. doi:10.1021/je200388s
32. Bankole DT, Inyinbor AA, Oluyori AP, Arowolo MO. Adsorptive removal of synthetic food dyes using low-cost biochar: efficiency prediction, kinetics and desorption index evaluation. Bioresour. Technol. Rep. 2024;25:101709. doi:10.1016/j.biteb.2023.101709
33. Schio RR, Gonçalves JO, Mallmann ES, Pinto D, Dotto GL. Development of a biosponge based on luffa cylindrica and crosslinked chitosan for allura red AC adsorption. Int. J. Biological Macromol. 2021;192:1117–22. doi:10.1016/j.ijbiomac.2021.10.096
34. da Rosa Schio R, Cruz da Rosa B, Gonçalves Salau NP, Stoffels Mallmann E, Dotto GL. Fixed-bed Adsorption of allura Red dye on Chitosan/polyurethane Foam. Chem. Eng. & Technol. 2019;42(11):2434–42. doi:10.1002/ceat.201800749
35. Benettayeb A, Ghosh S, Usman M, Seihoub FZ, Sohoo I, Chia CH, Sillanpää M. Some Well-known Alginate and chitosan Modifications used in Adsorption: A Review. Water. 2022;14(9):1353. doi:10.3390/w14091353
36. Boamah PO, Huang Y, Hua M, Zhang Q, Wu J, Onumah J, Sam-Amoah LK, Boamah PO. Sorption of heavy metal ions onto carboxylate chitosan derivatives—A mini-review. Ecotoxicol Environ Saf. 2015;116:113–120. doi:10.1016/j.ecoenv.2015.01.012
37. Reyna G. SD, Yedidia VP, María del Rosario MM, Jaime LC, Dalia I. SM, Ma. A. CM. Behavior of the adsorption of allura Red dye by chitosan beads and nanoparticles. Nanotechnol Environ Eng. 2023;8(1):49–62. doi:10.1007/s41204-022-00268-8
38. Dotto GL, Vieira MLG, Esquerdo VM, Pinto LAA. Equilibrium and thermodynamics of azo dyes biosorption onto spirulina platensis. Braz J Chem Eng. 2013;30(1):13–21. doi:10.1590/S0104-66322013000100003
39. Benettayeb A, Usman M, Tinashe CC, Adam T, Haddou B. A critical review with emphasis on recent pieces of evidence of moringa oleifera biosorption in water and wastewater treatment. Environ Sci Pollut Res. 2022;29(32):48185–209. doi:10.1007/s11356-022-19938-w
40. Benettayeb A, Hadj Brahim M, Lal B, Al-Farraj S, Belkacem M, John Masamvu M, Haddou B, Ali Alkahtane A, Chia C, Sillanpaa M, Ghosh S, Hosseini-Bandegharaei A. Insights into logical method selection for modification of chitosan and alginate towards the adsorption of heavy metal ions: a review. Environ Technol Rev. 2024;13(1):398–20. doi:10.1080/21622515.2024.2354519
41. Pestov A, Bratskaya S. Chitosan and its Derivatives as highly Efficient polymer Ligands. Molecules. 2016;21(3):330. doi:10.3390/molecules21030330
42. Benettayeb A, Haddou B. New biosorbents based on the seeds, leaves and husks powder of moringa oleifera for the effective removal of various toxic pollutants. Int J Environ Anal Chem. 2023;103(18):6859–84. doi:10.1080/03067319.2021.1963714
43. Şen NE, Şenol ZM. Effective removal of allura red food dye from water using cross-linked chitosan-diatomite composite beads. Int J Biological Macromol. 2023;253:126632. doi:10.1016/j.ijbiomac.2023.126632
44. Gonçalves JO, Silva KA, Dotto GL, Pinto LAA. Adsorption kinetics of dyes in single and binary Systems using Cyanoguanidine-crosslinked Chitosan of different Deacetylation Degrees. J Polym Environ. 2018;26(6):2401–2409. doi:10.1007/s10924-017-1133-z
45. Wang J, Chen C. Chitosan-based biosorbents: modification and application for biosorption of heavy metals and radionuclides. Bioresour. Technol. 2014;160:129–41. doi:10.1016/j.biortech.2013.12.110
46. Shankar S, Joshi S, Srivastava RK. A review on heavy metal biosorption utilizing modified chitosan. Environ Monit Assess. 2023;195(11). doi:10.1007/s10661-023-11963-7
47. Ali HB, Mansour R. Modeling of the adsorption of acidic dyes by chitosan using both kinetic and thermodynamic comparisons. J Text Inst. 2024;115(11):2214–23. doi:10.1080/00405000.2023.2283822
48. Skorik YA, Pestov AV, Kodess MI, Yatluk YG. Carboxyalkylation of chitosan in the gel state. Carbohydr Polym. 2012;90(2):1176–1181. doi:10.1016/j.carbpol.2012.06.072
49. Adi Sulianto A, Adiyaksa IP, Wibisono Y, Khan E, Ivanov A, Drannikov A, Ozaltin K, Di Martino A. From fruit Waste to hydrogels for agricultural Applications. Clean Technol. 2023;6(1):1–17. doi:10.3390/cleantechnol6010001
50. Rahman MS, Rana MM, Spitzhorn LS, Akhtar N, Hasan MZ, Choudhury N, Fehm T, Czernuszka JT, Adjaye J, Asaduzzaman SM. Fabrication of biocompatible porous scaffolds based on hydroxyapatite/collagen/chitosan composite for restoration of defected maxillofacial mandible bone. Prog Biomater. 2019;8(3):137–54. doi:10.1007/s40204-019-0113-x
51. Murcia-Salvador A, Pellicer JA, Fortea MI, Gómez-López VM, Rodríguez-López MI, Núñez-Delicado E, Gabaldón JA. Adsorption of direct Blue 78 using Chitosan and cyclodextrins as Adsorbents. Polymers. 2019;11(6):1003. doi:10.3390/polym11061003
52. Ho Y. The kinetics of sorption of divalent metal ions onto sphagnum moss peat. Water Res. 2000;34(3):735–742. doi:10.1016/s0043-1354(99)00232-8
53. Weber WJ, Morris JC. Kinetics of adsorption on carbon from solution. J. Sanit. Eng. Div. 1963;89:31–60.

54. Bensalah J. Removal of the textile dyes by a resin adsorbent polymeric: insight into optimization, kinetics and isotherms adsorption phenomenally. Inorg Chem Commun. 2024;161:111975. doi:10.1016/j.inoche.2023.111975
55. Wang Y, Wang C, Huang X, Zhang Q, Wang T, Guo X. Guideline for modeling solid-liquid adsorption: Kinetics, isotherm, fixed bed, and thermodynamics. Chemosphere. 2024;349:140736. doi:10.1016/j.chemosphere.2023.140736
56. Murcia-Salvador A, Pellicer JA, Fortea MI, Gómez-López VM, Rodríguez-López MI, Núñez-Delicado E, Gabaldón JA. Adsorption of direct Blue 78 using Chitosan and cyclodextrins as Adsorbents. Polymers. 2019;11(6):1003. doi:10.3390/polym11061003
57. Debord J, Chu KH, Harel M, Salvestrini S, Bollinger JC. Yesterday, Today, and Tomorrow. evolution of a sleeping Beauty: the Freundlich Isotherm. Langmuir. 2023;39(8):3062–3071. doi:10.1021/acs.langmuir.2c03105
58. Yetgin S, Amlani M. Agricultural low-cost waste adsorption of methylene blue and modelling linear isotherm method versus nonlinear prediction. Clean Technol Environ Policy. 2024. doi:10.1007/s10098-024-02928-6
59. Skatova AV, Boroda AV, Privar YO, Slobodyuk AB, Kantemirova EV, Bratskaya SY. Hydrogels of N-(2-Carboxyethyl)chitosan with Vanillin. Polym Sci Ser B. 2022;64(5):699–706. doi:10.1134/s1560090422700361
60. Ibrahim HM, Mostafa M, Kandile NG. Potential use of N-carboxyethylchitosan in biomedical applications: Preparation, characterization, biological properties. Int J Biolog Macromol. 2020;149:664–671. doi:10.1016/j.ijbiomac.2020.01.299
61. Bratskaya S, Skatova A, Privar Y, Boroda A, Kantemirova E, Maiorova M, Pestov A. Stimuli-responsive Dual Cross-linked N-carboxyethylchitosan Hydrogels with tunable Dissolution Rate. Gels. 2021;7(4):188. doi:10.3390/gels7040188
62. Benettayeb A, Masamvu JM, Chitepo RM, Haddou B, Sillanpaa M, Ghosh S. Facile fabrication of new bioadsorbents from moringa oleifera and alginate for efficient removal of uranium(VI). J Radioanal Nucl Chem. 2024;333(5):2369–87. doi:10.1007/s10967-024-09470-1
63. B. Guo, J. Qu, X. Zhao and M. Zhang, Degradable Conductive Self-Healing Hydrogels Based on Dextran-Graft-Tetraaniline and N-Carboxyethyl Chitosan as Injectable Carriers for Myoblast Cell Therapy and Muscle Regeneration, Acta Biomater., 2019, 84, 180–93. doi:10.1016/j.actbio.2018.12.00
64. Korel A, Samokhin A, Zemlyakova E, Pestov A, Blinova E, Zelikman M, Tkachenko V, Bets V, Kretien S, Arzhanova E, Litvinova E. A carboxyethylchitosan Gel Cross-linked with glutaraldehyde as a candidate Carrier for biomedical Applications. Gels. 2023;9(9):756. doi:10.3390/gels9090756
65. Zhao H, Zhang Y, Zhou C, Zhang C, Liu B. Engineering pH responsive carboxyethyl chitosan and oxidized pectin -based hydrogels with self-healing, biodegradable and antibacterial properties for wound healing. Int J Biolog Macromol. 2023;253:127364. doi:10.1016/j.ijbiomac.2023.127364
66. Yang S, Dong Q, Yang H, Liu X, Gu S, Zhou Y, Xu W. N-carboxyethyl chitosan fibers prepared as potential use in tissue engineering. Int J Biolog Macromol. 2016;82:1018–1022. doi:10.1016/j.ijbiomac.2015.10.078
67. Horathal Pedige MP, Sugawara A, Uyama H. Multifunctional chitosan Nanofiber-based Sponge materials Using Freeze–thaw and Post-Cross-linking Method. ACS Omega. 2024. doi:10.1021/acsomega.4c04317
68. Waresindo WX, Luthfianti HR, Priyanto A, Hapidin DA, Edikresnha D, Aimon AH, Suciati T, Khairurrijal K. Freeze–thaw hydrogel fabrication method: basic principles, synthesis parameters, properties, and biomedical applications. Mater Res Express. 2023;10(2):024003. doi:10.1088/2053-1591/acb98e
69. Georgin J, Stracke Pfingsten Franco D, Gindri Ramos C, Nguyen Tran H, Benettayeb A, Imanova G, Ali I. Recent advances in removing glyphosate herbicide and its aminomethylphosphonic acid metabolite in water. J Mol Liq. 2024;402:124786. doi:10.1016/j.molliq.2024.124786